Biomaterials Science

ROYAL SOCIETY OF CHEMISTRY

REVIEW

View Article Online
View Journal | View Issue

Cite this: *Biomater. Sci.*, 2025, **13**, 2628

Ultrasound-activated inorganic nanomaterials to generate ROS for antibacterial applications

Gaoquan Zheng,[a] Zhongmin Tang *[b,c] and Feng Peng *[a]

Given the global overuse and misuse of antibiotics, the problem of antibiotic resistance has become increasingly severe, necessitating the urgent development of innovative therapeutic strategies to address bacterial infections. In recent years, nanomaterial-mediated sonodynamic therapy (SDT) has emerged as a promising alternative treatment. This strategy works by generating reactive oxygen species (ROS) to inhibit or kill bacteria, thereby avoiding the risk of antibiotic resistance. This review explores the various mechanisms by which ROS exert antibacterial effects and examines the different methods of generating ROS. It provides an overview of the diverse nanomaterials applied in SDT in recent years, including two-dimensional materials, metal–organic frameworks (MOFs), heterojunctions, and surface-modified bulk materials. Additionally, it discusses other types of nanomaterials such as metal oxides and piezoelectric materials, while also highlighting their specific therapeutic applications in treating infections like skin infections and osteomyelitis. At the conclusion of the review, the development of nanomaterial-mediated SDT is discussed in terms of both its potential and challenges. The article offers valuable theoretical insights and practical references for the preparation of the nanomaterials required for this antibiotic-free therapeutic approach, and proposes new directions for future research aimed at addressing the growing issue of antibiotic resistance.

Received 23rd January 2025,
Accepted 9th April 2025

DOI: 10.1039/d5bm00121h

rsc.li/biomaterials-science

1. Introduction

With the development of human medicine, bacterial infection is still one of the vital causes of death. Since the discovery of penicillin by Alexander Fleming in 1928, the mortality rate of bacterial infections has been controlled.[1] The advent of antibiotics has led to a significant reduction in mortality rates, decreasing by 25–30% for both community-acquired and healthcare-associated pneumonia, 75% for endocarditis, 60% for meningeal or cerebral infections, and 11% for cellulitis.[2,3] However, over the years, the widespread misuse of antibiotics has led to the emergence of antibiotic-resistant bacteria, such as methicillin-resistant *Staphylococcus aureus* (MRSA), vancomycin-resistant enterococci (VRE), and vancomycin-resistant *Staphylococcus aureus* (VRSA). These bacteria develop resistance to existing antibiotics through various mechanisms, rendering many traditional antibiotics ineffective.[4–6] Therefore, to prevent the continued rise of antibiotic resistance and to treat infections caused by these resistant bacteria, it is crucial to urgently explore alternative non-antibiotic methods for combating bacterial infections.

Traditional non-antibiotic treatments for bacterial infections, such as plant extracts[7] and probiotic therapies,[8] are limited in their scope of application and suffer from a lack of standardization. In recent years, antibacterial therapies based on physical stimuli have garnered widespread attention as alternatives to antibiotics, becoming a major focus of antimicrobial research.[9] Examples include photodynamic therapy,[10,11] sonodynamic therapy,[12] electrodynamic therapy,[13] and thermodynamic therapy.[14,15] Among these, sonodynamic therapy (SDT) is a therapeutic approach that combines non-toxic sensitizing agents with low-intensity ultrasound to achieve treatment of both superficial and deep-targeted tissue diseases. Under ultrasound stimulation, these sonosensitizers, typically composed of nanomaterials, generate reactive oxygen species (ROS), thereby inducing site-specific cytotoxic effects.[16] This approach offers the advantages of broad-spectrum antibacterial activity and a low risk of resistance development.[12,17] Herein, we first discuss the antibacterial mechanism of ROS and their source, and then review recent advancements in the application of nanomaterials SDT capability for antibacterial purposes (Fig. 1).

[a]*Medical Research Institute, Department of Orthopedics, Guangdong Provincial People's Hospital, Guangdong Academy of Medical Sciences, Southern Medical University, Guangzhou, Guangdong 510080, China. E-mail: pengfeng@gdph.org.cn*
[b]*Department of Cardiology, Shanghai Tenth People's Hospital, School of Medicine, Tongji University, Shanghai, 200072, P. R. China.*
E-mail: zhongmintang@tongji.edu.cn
[c]*Shanghai Frontiers Science Center of Nanocatalytic Medicine, School of Medicine, Tongji University, Shanghai, 200072, P. R. China.*
E-mail: zhongmintang@tongji.edu.cn

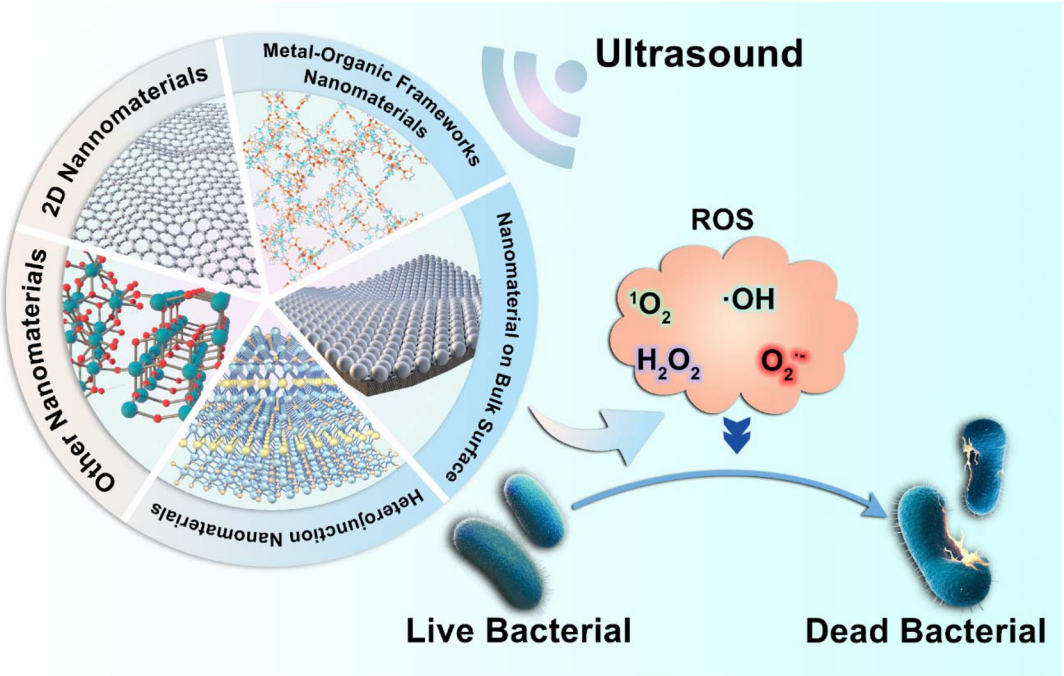

Fig. 1 Schematic illustration of nanomaterial-mediated SDT antibacterial mechanism.

2. Antibacterial mechanism of ROS and the way to generate ROS

2.1 Antibacterial mechanism of ROS

ROS, encompassing both radical and non-radical oxygen derivatives such as superoxide anion ($O_2^{\bullet-}$), hydrogen peroxide (H_2O_2), hydroxyl radical ($^{\bullet}OH$), and singlet oxygen ($^1O_2$), are known for their high chemical reactivity due to unpaired electrons.[18,19] These ROS can exert antibacterial effects against various pathogens through multiple pathways.[20]

In the process of combating bacteria, ROS exert their antibacterial effects primarily by reacting with bacterial DNA, proteins, cell membranes, and lipids, resulting in irreversible damage and disruption of bacterial growth.[21] These ROS can induce the formation of oxidative products, such as 8-hydroxyguanine (8-oxoG),[22] through oxidation, leading to base mismatches, mutations, and DNA strand breaks. This disrupts the normal processes of DNA replication and transcription in bacteria, thereby inhibiting their growth and reproduction. ROS can also interact with sulfur-containing amino acids, such as cysteine, causing thiol oxidation and the formation of disulfide bonds, which leads to protein denaturation, weakening the bacterial metabolic and defense mechanisms, and ultimately resulting in a loss of function.[23] On bacterial cell membranes, ROS can react with membrane lipids, especially unsaturated fatty acids, leading to the formation of lipid peroxidation products such as malondialdehyde (MDA).[24,25] These reactive products can damage the membrane structure, causing leakage of intracellular contents and loss of function, which facilitates the entry of nanomaterials and ROS into the bacterial cell interior, thereby enhancing their antibacterial effects.[21]

In addition to the mechanisms mentioned above, among these ROS, $O_2^{\bullet-}$ is often regarded as the "primary" radical formed during the ROS generation cascade. Upon acquiring a single electron, molecular oxygen initially converts to $O_2^{\bullet-}$. Subsequently, $O_2^{\bullet-}$ can undergo dismutation catalyzed by superoxide dismutase (SOD) to produce H_2O_2 and molecular oxygen. Under certain conditions, $O_2^{\bullet-}$ can also participate in further reactions to form highly oxidizing species such as the $^{\bullet}OH$. Notably, compared to other ROS, the neutral nature of H_2O_2 enables it to more readily cross cell membranes and interact with intracellular components. Inside bacterial cells, hydrogen peroxide interferes with essential metabolic processes by oxidizing iron-sulfur cluster enzymes, such as dehydrogenases, and other iron-containing enzymes, leading to the loss of bacterial viability.[21,23] Among these ROS, $^{\bullet}OH$ are considered one of the most potent biological oxidants, with their exceptionally high reactivity and non-selectivity being key factors behind their antibacterial efficacy.[26,27] $^1O_2$ exhibits high selectivity, primarily reacting with molecules containing double bonds, such as unsaturated fatty acids and aromatic compounds. This selective reactivity makes $^1O_2$ highly effective in oxidizing cell membranes, proteins, and certain nucleic acids, leading to targeted damage at specific cellular sites. This characteristic enables $^1O_2$ to play a critical role in localized treatments, such as tumor cell destruction.[28–30] In antibacterial pathways, these ROS work synergistically to achieve enhanced antibacterial effects.

2.2 Sources and mechanisms of reactive oxygen species generation

As discussed previously, ROS exert bactericidal effects through various mechanisms. These ROS are primarily generated through Fenton reaction, Fenton-like reaction, extracellular stimuli, and drug-induced processes.

The Fenton reaction refers to the process in which ferrous ions (Fe^{2+}) decompose H_2O_2 to generate $^{\bullet}OH$ and other ROS.[31] The reaction is typically represented as follows:

$$H_2O_2 + Fe^{2+} \rightarrow Fe^{3+} + OH^- + {}^{\bullet}OH$$

Reactions similar to the Fenton reaction, but without the involvement of Fe^{2+}, are referred to as Fenton-like reactions. The key characteristic of these reactions is the use of other metal ions, such as copper[32] and cobalt,[33] to replace ferrous ions in generating ROS. Fenton-like reactions typically exhibit broader catalytic selectivity compared to traditional Fenton reactions, and through the synergistic action of different metal ions, they can effectively eliminate a wide range of bacteria.

Under various extracellular stimuli, different types of ROS can be generated. For instance, in photodynamic therapy, photosensitizers absorb light and react with oxygen to produce $^1O_2$. Immune cells, when activated by external signals such as pathogens or cellular damage, generate ROS to eliminate the invading organisms. Additionally, exposure to high-energy radiation, such as ultraviolet (UV) light, can induce ROS production, including hydrogen peroxide, through interactions with water molecules.

Some antibiotics can also generate ROS. For example, quinolone drugs induce ROS generation by binding to topoisomerases, forming DNA damage complexes that hinder DNA replication.[34] Additionally, 2-nitroimidazole compounds (such as IAZA and FAZA) accumulate under hypoxic conditions and are reduced within the cells to their active forms. These compounds then release electrons, which react with molecular oxygen, leading to the generation of superoxide, hydrogen peroxide, and other ROS.[35]

Emerging SDT, which generates ROS through the interaction of nanomaterials with ultrasound, offers a promising strategy for antibacterial treatment. This therapy produces ROS through various mechanisms, including cavitation effects[36] and electron–hole pair formation.[37] The cavitation effect occurs when microbubbles formed in a liquid under ultrasonic irradiation rapidly expand and collapse, creating intense localized pressure and temperature. This process accelerates molecular collisions and facilitates interactions between the material and its surrounding environment, resulting in the generation of a substantial quantity of ROS. Under ultrasonic stimulation, certain nanomaterials generate electron–hole pairs (e^-/h^+), where the excited-state electrons (e^-) exhibit strong reducing properties, enabling them to react with oxygen molecules in water to produce $O_2^{\bullet-}$. Meanwhile, the holes (h^+) possess strong oxidative properties and can react with OH^- in water to generate $^{\bullet}OH$.[38,39] SDT not only efficiently generates ROS and reduces the development of bacterial resistance, but also offers several advantages over other ROS-generating methods. These advantages include the ability to focus on localized antibacterial effects without damaging normal cells, non-invasive treatment of deep tissues, dynamic control of ROS production to maximize antibacterial efficacy, and synergistic interactions with nanomaterials to enhance antibacterial activity. The following sections will provide a detailed review of these emerging nanomaterials.

3. Inorganic nanomaterials response to ultrasound activation to generate ROS for antibacterial therapy

Ultrasound intensity typically ranges from 0.5 W cm^{-2} to 1.5 W cm^{-2} when activating inorganic nanomaterials to generate ROS, with a frequency commonly set at 1 MHz and a duration ranging from 10 to 20 minutes. This range of intensity is effective in ensuring ROS production while minimizing damage to normal tissues. In this review, we categorize these inorganic nanomaterials into five groups: two-dimensional nanomaterials, metal–organic framework nanomaterials, heterojunction nanomaterials, other nanomaterials, and nanomaterials on bulk surfaces.

3.1 Two-dimensional nanomaterials

Two-dimensional (2D) nanomaterials refer to materials that have significant extension in two dimensions while being extremely thin in the third dimension. Due to their unique physicochemical properties, 2D nanomaterials have shown considerable advantages as biomaterials. Compared to other materials, 2D nanomaterials offer not only strong mechanical stability and good biocompatibility but also efficient electron transport capacity.[40,41] Materials such as graphene,[42] black phosphorus,[43] and transition metal dichalcogenides (TMDs)[44,45] typically exhibit unique electronic properties, including high conductivity and high electron mobility, which enable them to efficiently transfer electrons under ultrasound stimulation.[46] This, in turn, promotes the generation of ROS, thereby achieving antimicrobial effects.

Stanene, a 2D nanomaterial composed of tin atoms, boasts an exceptionally high specific surface area and outstanding electron transport properties, making it highly promising for use in SDT for antibacterial applications. In the study by Tao *et al.*,[47] under ultrasound activation, the stanene nanosheets absorb acoustic energy and convert it into thermal energy. This thermal effect excites the electrons in stanene, elevating them to high-energy states. Due to the high specific surface area and excellent electron transport capacity of two-dimensional materials, these excited electrons can quickly propagate and migrate. This results in the interaction of the excited-state electrons with oxygen molecules, generating $^1O_2$. Meanwhile, the holes in stanene, which possess strong oxidative properties, can react with hydroxide ions in water, producing $^{\bullet}OH$. In this study, the material demonstrated antimicrobial rates of

99.80% and 99.50% against MRSA and *S. aureus*, respectively, upon ultrasound stimulation. The researchers developed a hydrogel based on stanene nanosheets (SnNSs) to treat wound bacterial infections, promote wound healing, and reduce inflammatory responses[47] (Fig. 2A). Chen *et al.* applied the same SDT approach and principles to promote ROS generation by stanene, with a distinct focus on cancer therapy in their research.[48]

Compared to stanene, the MXenes family have found broader application in SDT due to its excellent biocompatibility and functionalization potential. MXenes are two-dimensional nanomaterials composed of transition metal carbides, which have gained increasing attention owing to their unique surface functional groups (such as –OH, –O, –F) and dual metallic-ceramic properties.[49] In SDT, this material not only generates ROS through the cavitation effect induced by ultrasound, but also forms e^-/h^+ on its surface. The abundance of active functional groups on the material's surface not only enhances its hydrophilicity but also provides rich chemical active sites, thereby improving the efficiency of ROS generation. Ma *et al.* developed a two-dimensional material, Nb_2C, from the MXenes family. Under ultrasonic irradiation, Nb_2C nanosheets on the nanoplatform formed Schottky junctions with porphyrin-based metal–organic frameworks, facilitating rapid charge transfer. This charge transfer suppressed the recombination of electron–hole pairs, leading to the generation of abundant ROS for antibacterial activity, achieving an antibacterial rate of 98.64% ± 0.25% against MRSA.[39] Furthermore, an *in vivo* study using a bone marrow infection model of MRSA demonstrated that the HNTM/Nb_2C nanoplatform exhibited remarkable antibacterial properties and promoted bone regeneration, highlighting its potential for both infection treatment and bone healing(1.5 W cm^{-2},1 MHz, 20 min)[39] (Fig. 2B). Song *et al.* synthesized a high-entropy

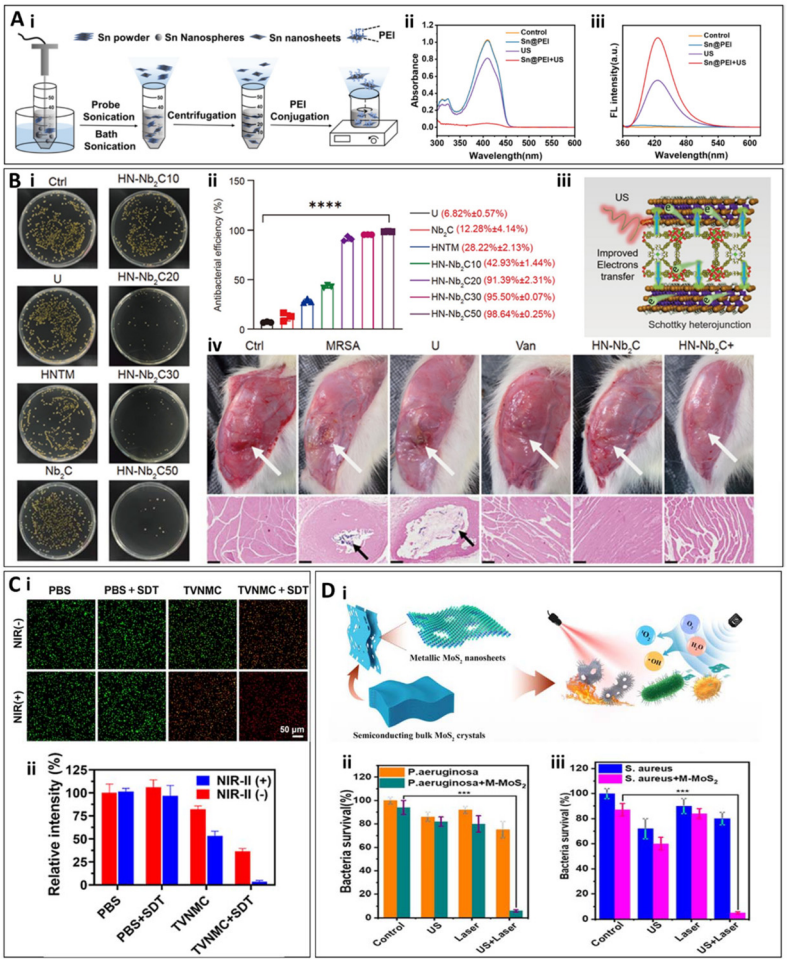

Fig. 2 (A) (i) Schematic diagram of the preparation of SnNSs and Sn@PEI. (ii) Absorption spectra of DPBF for $^1O_2$ irradiation. detection. (iii) Fluorescent spectra showing $^{\bullet}OH$ generation with TA.[47] Copyright©2023, Elsevier. (B) (i) Spread plate images of MRSA of the varied materials with or without US irradiation for 15 min. (ii) Antibacterial efficiencies of different samples, based on the spread plate pictures. (iii) ROS generation mechanism. (iv) Leg images of infected sites. Abscesses are highlighted with white arrows. Gram staining of muscle in infected sites. MRSA are indicated with black arrows. Scale bar: 500 μm.[39] Copyright©2023, Science China Press. (C) Bacterial viability and mortality staining images of TVNMC (i) and quantitative counting graph (ii).[50] Copyright©2024, Elsevier. (D) (i) Preparation and mechanism diagram of MoS_2. (ii) and (iii) The antibacterial rate of MoS_2 against *S. aureus* and *P. aeruginosa*.[51] Copyright©2023, Springer Nature.

MXene (HEM), specifically TVNMC MXene. In contrast to the study by Ma *et al.*, this material can respond to both ultrasonic and NIR-II stimuli, synergistically generating ROS for antibacterial activity. In vitro antibacterial results demonstrated that, in this photothermal-enhanced sonodynamic antibacterial therapy, the antibacterial rate against MRSA reached 99.60%, surpassing the efficacy of ultrasound stimulation alone. Furthermore, *in vivo* experiments confirmed that TVNMC MXene effectively eliminated MRSA and its biofilm, while promoting wound healing without causing noticeable abnormalities in mouse tissues (1.0 W cm^{-2}, 1 MHz, 20 min)[50] (Fig. 2C).

MoS_2 exhibits a mechanism of action similar to that of TVNMC MXene, demonstrating excellent light absorption in the NIR spectrum. This allows it to synergize with NIR light-induced thermal effects and ultrasound-triggered energy conversion, further enhancing the generation of ROS. In the study by Chen *et al.* These MoS_2 nanosheets possess tunable metal–semiconductor phase transition properties. Under ultrasound stimulation in sonodynamic therapy, MoS_2 can transition from a semiconductor phase to a metallic phase, which enhances its conductivity and improves its ability to generate ROS upon ultrasound activation. In this study, *in vitro* and *in vivo* antibacterial experiments were conducted against *S. aureus* and *P. aeruginosa*, with nearly 100% antibacterial efficacy observed under the synergistic photothermal and sonodynamic effects. Additionally, the treatment demonstrated significant efficacy in wound infection and healing (1.0 W cm^{-2}, 1 MHz, 20 min)[51] (Fig. 2D).

3.2 Metal–organic frameworks nanomaterials

Metal–organic frameworks (MOFs) are highly ordered three-dimensional structures formed by metal ions or metal clusters coordinated with organic ligands. Due to their high specific surface area, tunable pore structure, and excellent chemical stability, MOFs are widely applied in various fields of life sciences.[52]

The primary advantage of MOFs lies in their ability to not only respond to ultrasound for antibacterial activity, but also to selectively design their porous structure to control the rate of ROS release, thereby modulating cellular behavior for therapeutic purposes. In the study by Ma *et al.*, a Janus-ROS therapeutic system was proposed,[53] in which the MOF was designed with one side incorporating an ALN-mediated defective metal–organic framework that exhibits ultrasound-activated antibacterial properties. Under high-intensity ultrasound stimulation, this side rapidly generates a substantial amount of ROS, effectively exerting antibacterial effects. The other side, in contrast, generates a small amount of ROS under low-intensity ultrasound stimulation, which modulates the behavior of osteocytes. This is achieved by influencing transcription factors such as FOXO, thus promoting the expression of osteogenic genes, stimulating osteoblast differentiation, and facilitating bone tissue repair.[53] Meanwhile, experimental results demonstrated that the material exhibited an antibacterial efficiency of 98.97% against MRSA (1.5 W cm^{-2}, 1 MHz, 15 min)[53] (Fig. 3A).

Furthermore, the porous structure of MOFs allows them to generate ROS *via* cavitation effects under ultrasound, thereby achieving antibacterial activity. Modifying with other elements further enhance the efficiency of ROS production. In the study by Sun *et al.*, a designed Ag-modified multi-metallic organic framework (Ag@UT) was synthesized. This material was prepared by incorporating tetra(4-carboxyphenyl) porphyrin (TCPP) into a zirconium-based MOF (UiO-66), followed by *in situ* reduction of silver nitrate ($AgNO_3$) on its surface to grow silver nanoparticles (Ag NPs). This structure resulted in a reduction of the energy band gap of the resulting multi-metallic MOF (UT) from 3.45 eV to 2.58 eV. Upon *in situ* growth of Ag NPs, the band gap of Ag@UT was further reduced to 2.11 eV, facilitating easier generation of electron–hole pairs upon ultrasound excitation to produce ROS (Fig. 3B). In the Ag@UT structure, electrons in UT spontaneously flow toward Ag NPs until equilibrium is reached, forming a Schottky barrier. More long-lived electrons transfer energy to surrounding $^3O_2$ molecules, generating $^1O_2$. The Schottky barrier described here and the Schottky junction formed in the HNTM/Nb2C nanoplatform function similarly by leveraging the difference in energy levels between materials to control the flow and distribution of electrons, thereby enhancing the generation of ROS. However, there is a distinction in their mechanisms: the Schottky barrier in Ag@UT promotes the accumulation of electrons in Ag NPs, which then react with surrounding oxygen molecules to produce ROS. In contrast, the Schottky junction in the latter system enhances ROS production by inhibiting the recombination of e^-/h^+. These nuanced differences in electron behavior at the material interfaces are pivotal for optimizing the sonodynamic effects in biomedical applications, particularly in antimicrobial and tissue repair strategies. This study confirmed the antibacterial efficacy of the material under ultrasound against *S. aureus*, with an antibacterial efficiency exceeding 99% at an Ag@UT concentration of 256 μg ml^{-1}. Furthermore, in a *Staphylococcus aureus*-infected wound model, the material exhibited therapeutic effects by treating the infection and promoting wound healing (1.0 W cm^{-2}, 1 MHz, 10 min).[54] Similar to their work, Zheng *et al.* synthesized a CeTCPP-Au complex through a solvothermal reaction, where TCPP (along with ($(NH_4)_2[Ce(NO_3)_6]$)) was used to prepare the material, with TCPP serving as the sonosensitizer. Gold nanoparticles (Au NPs) were then loaded onto CeTCPP *via in situ* reduction of $HAuCl_4$ to obtain CeTCPP-Au. This material exhibits similar characteristics, where the interface between Au NPs and CeTCPP forms a Schottky barrier due to the difference in Fermi levels, which inhibits electron backflow to CeTCPP and promotes electron–hole pair separation, thereby enhancing the sonodynamic effect to generate ROS (Fig. 3C). *In vitro* antibacterial experiments showed that CeTCPP-Au exhibited antibacterial efficiencies of 99.73 ± 0.05% against *S. aureus* and 99.16 ± 0.29% against *E. coli*. Furthermore, in an *in vivo* rat model of osteomyelitis, treatment with CeTCPP-Au in combination with ultrasound resulted in reduced inflammation, as evidenced by a decrease in interleukin-6 (IL-6) levels. Blood tests showed a reduction in white blood cell (WBC), lymphocyte (Lymph), gra-

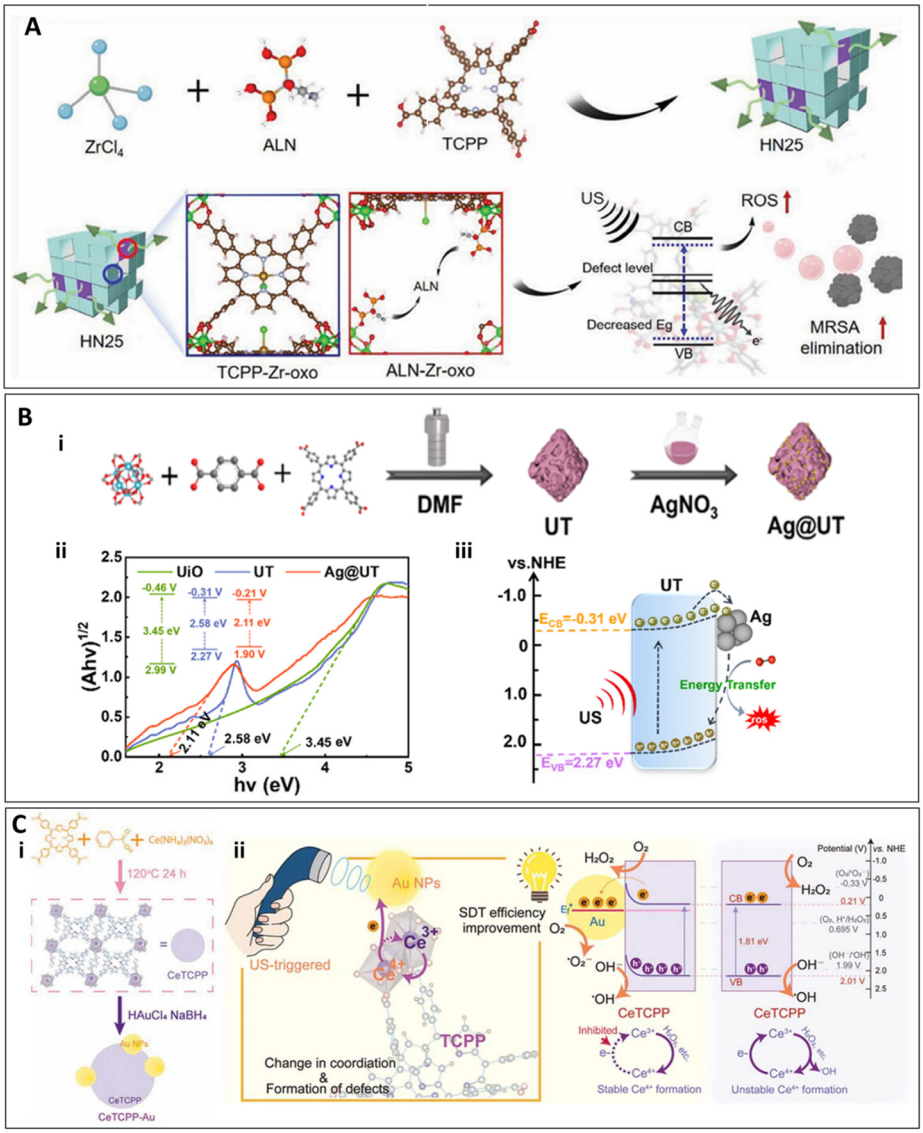

Fig. 3 (A) Preparation and mechanism of action of HN25.[53] Copyright©2023, Wiley-VCH. (B) Schematic illustration of the preparation procedure of Ag@UT (i) and (ii) band gaps and energy level diagram (insets) of UiO, UT and Ag@UT, (iii) US-induced sono-catalytic mechanism of Ag@UT.[54] Copyright©2024, Elsevier. (C) (i) The preparation of CeTCPP-Au. (ii) Schematic illustration of the mechanism of the defect formation in CeTCPP-Au and the processes of ROS generation.[55] Copyright©2023, Wiley-VCH.

nulocyte (Gran), red blood cell (RBC), hemoglobin (HGB), hematocrit (HCT), and platelet (PLT) counts, indicating a reduction in inflammation. Additionally, bacterial infection and inflammatory cell counts in the bone marrow were significantly reduced, with no obvious damage to major organs.[55] Although these two materials can also be classified as heterojunction nanomaterials, it is considered that their primary application leverages the unique mechanisms of MOFs. A detailed discussion on heterojunction nanomaterials will be presented in the following sections.

3.3 Heterojunction nanomaterials

Heterojunction nanomaterials refer to a class of materials formed by the combination of two or more different components, where the interface between these materials creates a unique structure. Compared to other materials discussed in this study, heterojunction materials present distinct advantages. Due to the differences in the electronic band structures of their constituent components—such as metal–semiconductor or semiconductor–semiconductor interfaces—heterojunctions can effectively generate built-in electric fields, thereby facilitating the efficient separation of electron–hole pairs.[38,56–60] This not only enhances the effective utilization of photoexcited charge carriers but also reduces the recombination of electrons and holes, improving catalytic efficiency. Under ultrasonic stimulation, this results in a significant increase in the generation of ROS, thereby enhancing the antimicrobial efficacy.[61]

Some heterojunction materials can promote ROS generation under ultrasonic stimulation by introducing defects that inhibit electron–hole recombination. A mechanism demonstrated in the study by Zeng *et al.*, which focused on a MOF based on porphyrin. By using acetic acid and benzoic acid as modulators during the hydrothermal synthesis, defects were introduced, creating a defective MOF (D-MOF) with a dual heterojunction structure (such as PCN-222/PCN-224). Among these, D-PCN-2 exhibited the best performance. *In vitro* experiments demonstrated that D-PCN-2 achieved an antibacterial efficiency of 93.05% against MRSA. In *in vivo* experiments, a rat model of MRSA-induced osteomyelitis was established. Through wound observation, blood analysis, histological staining (such as H&E and immunofluorescence staining), and

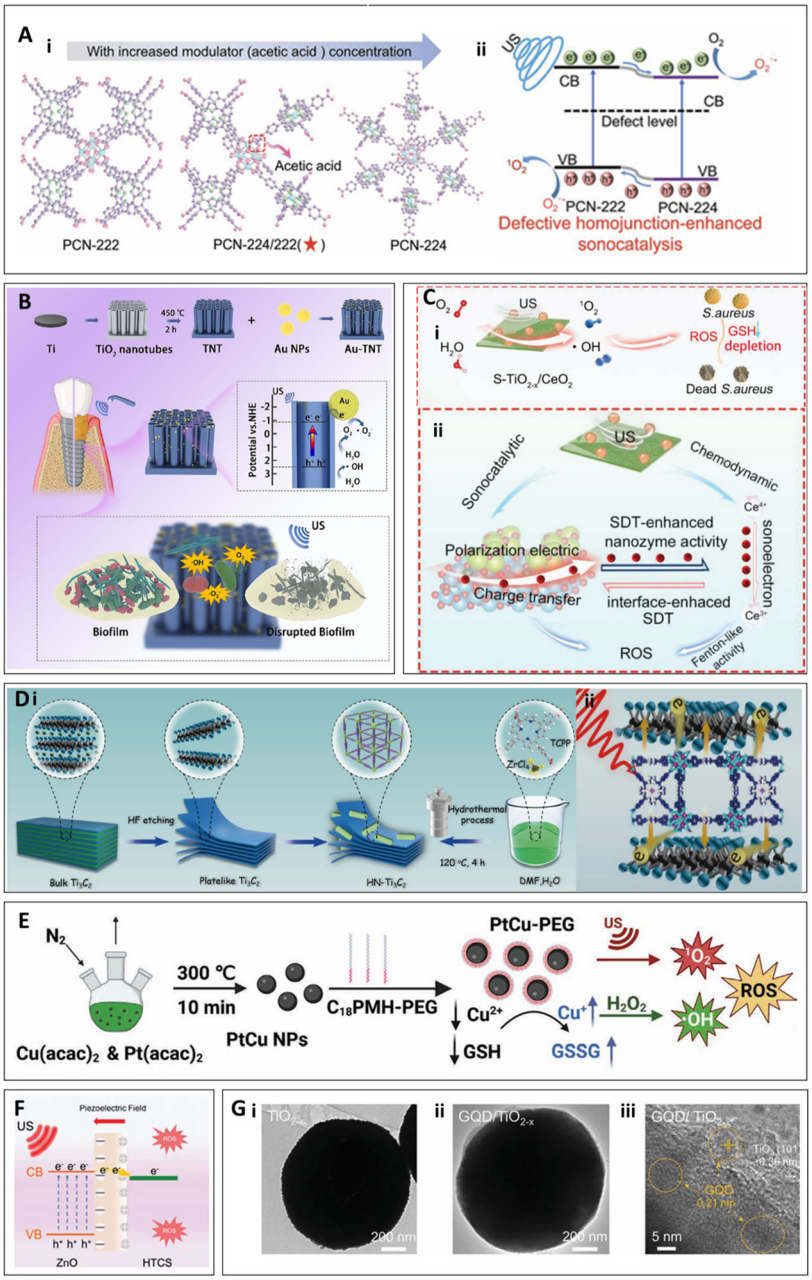

Fig. 4 (A) The transformation of the MOF heterojunction crystal structure (i) and the corresponding defect-enhanced sonocatalytic mechanism (ii).[62] Copyright©2022, Wiley-VCH. (B) Schematic depiction of the preparation process and enhanced SDT mechanism of Au-TNT.[57] Copyright©2023, Elsevier. (C) S-TiO_{2-x}/CeO_2 (i) ultrasonic antibacterial mechanism and (ii) mechanism of ROS generation through synergistic effects.[59] Copyright©2023, Wiley-VCH. (D) (i) Schematic illustration of the preparation procedure of Ti_3C_2, HNTM and HN-Ti_3C_2. (ii) antibacterial mechanism of HN-Ti_3C_2.[38] Copyright©2023, IVYSPRING. (E) Preparation and mechanism of action of PtCu-PEG NPs.[63] (F) Mechanism of ROS generation in ZnO@HTCS.[64] Copyright©2023, Wiley-VCH. (G) TEM and HRTEM images of TiO_{2-x} and GQD/TiO_{2-x}.[42] Copyright©2024, Wiley-VCH.

Micro-CT scanning, it was shown that D-PCN-2 effectively alleviated infection symptoms, reduced systemic inflammation, promoted bone regeneration, and successfully prevented bone destruction (1.5 W cm^{-2}, 1 MHz, 15 min)[62] (Fig. 4A).

Schottky heterojunctions refer to a specialized type of junction formed by the combination of metal and semiconductor materials, which plays a crucial role by generating an internal electric field. In the study by Li *et al.*, a gold-TiO_2 Schottky heterojunction was described, where the combination of metal and semiconductor generates an internal electric field that effectively promotes the separation of electron–hole pairs, thereby enhancing ROS generation efficiency under ultrasound stimulation (Fig. 4B). Antibacterial experiments were conducted against *P. gingivalis*, *F. nucleatum*, and *S. sanguinis*, showing antibacterial rates of 96.59%, 96.25%, and 95.31%, respectively. Additionally, *in vivo* experiments confirmed the material's promising efficacy in treating *peri*-implant infections under SDT.[57] Li *et al.* investigated a TiO_2-Ru-PEG Schottky heterojunction, similar to the gold-TiO_2 Schottky heterojunction. This heterojunction generates ROS through the same mechanism under ultrasound; however, their work focused on using this system for the treatment of bladder cancer.[58] As another example of a Schottky heterojunction, Wang *et al.* synthesized a defective S-doped TiO_2 and CeO_2 heterojunction (S-TiO_{2-x}/CeO_2). Unlike the previously discussed materials, under ultrasound stimulation, CeO_2 in S-TiO_{2-x}/CeO_2 exhibits mixed valence states of Ce^{3+}/Ce^{4+}. Ce^{4+} can deplete glutathione (GSH) in bacteria and react with H_2O_2 to generate ROS. Meanwhile, the ultrasound-induced sonoelectrons in S-TiO_{2-x}/CeO_2 can modulate the valence state transition between Ce^{3+} and Ce^{4+}, enhancing the efficacy of chemotherapeutic therapy (Fig. 4C). The heterojunction structure accelerates interface electron transfer, boosting SDT and achieving a synergistic effect between sonodynamic and chemotherapeutic mechanisms. The resulting ROS jointly contribute to bacterial cell death. Experimental results demonstrated that this material achieved an antibacterial efficiency of 99.30% against *S. aureus* under ultrasound and showed promising potential for the treatment of osteomyelitis caused by *S. aureus*.[59] A nanocomposite material named HN-Ti_3C_2, synthesized by Wang *et al.*, which forms a Schottky heterojunction between HNTM (Zr-porphyrin-based MOF hollow nanotubes) and Ti_3C_2 nanosheets, also demonstrates efficacy in the ultrasound-mediated treatment of osteomyelitis. Under ultrasound irradiation, HNTM generates electron–hole pairs, while Ti_3C_2 facilitates the rapid transfer of electrons, leading to the generation of a significant amount of ROS (Fig. 4D). Additionally, this heterojunction can generate piezoelectric currents under low-intensity ultrasound to promote bone regeneration. Experimental results showed that this material achieved an antibacterial efficiency of 99.75% against MRSA under ultrasound, and it exhibited promising effectiveness in treating MRSA-induced osteomyelitis while promoting bone regeneration (1.5 W cm^{-2}, 20 min).[38]

In addition, heterojunction materials can also optimize the combination of different substances' individual effects on bacteria to enhance antibacterial efficiency. For example, in the study by Cheng *et al.*, PtCu NPs (platinum–copper nanoparticles) were employed as ultrasound-activated nanosensitizers, which were subsequently modified with poly (maleic anhydride-*alt*-1-octadecene)-polyethylene glycol (C_{18}PMH-PEG) to yield PtCu-PEG NPs. This modification endowed the material with excellent biocompatibility, dispersibility, and enhanced ultrasound activity (Fig. 4E). The modification not only facilitated ROS generation but also synergistically enhanced the antibacterial effect by depleting glutathione. Experimental results demonstrated that, under 8 min of ultrasound irradiation, the material achieved antibacterial efficiencies of 99.60% against *E. coli* and 99.9% against *S. aureus*. This material showed significant advantages in treating wound infections and osteomyelitis caused by *S. aureus*.[63] On the other hand, heterojunction materials can also enhance the piezoelectric effect by combining different materials, thereby improving the efficiency of ultrasound-induced ROS generation (Fig. 4F). This mechanism has been demonstrated in the work of Guo *et al.* with their Glucose-derived carbon spheres loaded with zinc oxide (ZnO@HTCS),[64] which can be used to treat osteomyelitis caused by MRSA, exhibits an *in vitro* antibacterial efficiency of 99.79 ± 0.09% against MRSA (1.5 W cm^{-2}, 15 min).

Heterojunction materials can also optimize their catalytic performance, electronic conductivity, and ROS generation capability by incorporating carbon-based materials. In the work of Ying Qian *et al.*, a graphene quantum dots (GQDs) and TiO_{2-x} heterojunction was synthesized[42] (Fig. 4G). The graphene quantum dots enhance the catalytic efficiency of TiO_{2-x} by providing excellent electronic conductivity and light absorption capacity, enabling more efficient ROS generation under ultrasound conditions for antibacterial purposes. Moreover, this material demonstrated promising therapeutic effects in a mouse model of MRSA-infected skin wounds (1.0 W cm^{-2}, 20 min).[42]

3.4 Other nanomaterials

In addition to the materials mentioned above, other types of nanomaterials with specialized functions can also mediate SDT. Some metal oxide nanomaterials, such as TiO_2, exhibit excellent ultrasound responsiveness and favorable biocompatibility. In the study by Ouyang *et al.*, various crystalline phases of TiO_2 nanoparticles were analyzed, revealing that the II-type heterojunction of anatase-brookite TiO_2 (AB) exhibited the lowest adsorption and activation energy for O_2. This characteristic enabled efficient electron transfer to O_2, promoting the separation of electron–hole pairs, enhancing oxygen activation, and generating higher amounts of ROS (Fig. 5A). Building upon this, hyaluronic acid (HA) microneedles (MN) loaded with AB-type TiO_2 were synthesized. Experimental results demonstrated that AB-MN achieved an antibacterial efficiency of 99.94%. Under ultrasound irradiation, AB-MN effectively eradicated wound biofilms, alleviated inflammation, and promoted wound healing. This was evidenced by enhanced collagen formation, suppression of pro-inflammatory responses

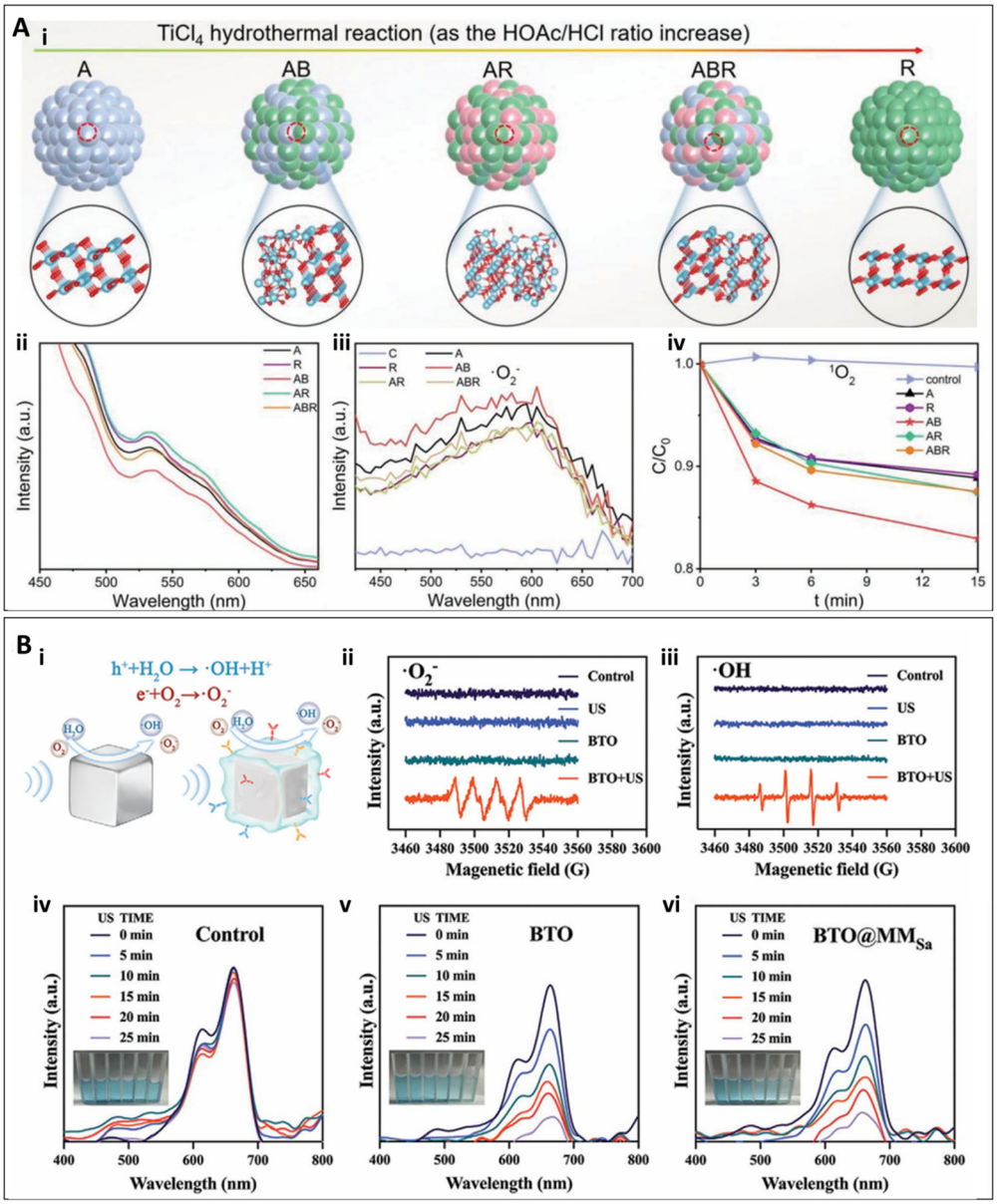

Fig. 5 (A) (i) Preparation of TiO_2 nanoparticles with different phase components. (ii) Photoluminescene spectra. (iii) Fluorescence intensity of NBT (for $O_2^{\bullet-}$) treated by samples under US for 15 min. (iv) Fluorescence intensity of DMA ($^1O_2$).[65] Copyright©2022, Wiley-VCH. (B) Piezocatalytic effects and ROS generation ability of BTO, BTO@MM0, and BTO@MMSa under US vibrations. (i) BTO and BTO@MMSa mediated piezoelectric effect for the generation of $O_2^{\bullet-}$ and $^{\bullet}OH$. (ii and iii) Electron spin resonance (ESR) spectra of $O_2^{\bullet-}$ and $^{\bullet}OH$ trapped by 5,5-dimethyl-1-pyrroline-*N*-oxide (DMPO) in methanol and water, respectively, under US irradiation. (iv–vi) UV-vis absorption spectra of methylene blue (MB) solutions in the control, BTO, and BTO@MMSa after varying durations of US stimulation. Inset pictures from left to right display the MB solution following different durations of US-triggered piezoelectric catalysis.[66] Copyright©2024, Wiley-VCH.

(such as reduced TNF-α expression), and stimulation of vascular tissue regeneration (as indicated by increased VEGF expression), providing an effective treatment for chronic wound infections (1.5 W cm^{-2}, 1 MHz, 15 min).[65]

The application of piezoelectric nanomaterials in SDT has emerged as an increasingly important area of research. These materials generate built-in electric fields under ultrasound stimulation, thereby promoting the production of ROS. Moreover, while exhibiting favorable biocompatibility, piezoelectric nanomaterials can be modified to achieve specific antibacterial objectives, such as minimizing damage to healthy tissues.[67] For example, in the study by Qian *et al.*, a piezo-catalytic nanomist (BTO@MMSa) pre-activated by macrophage membranes was developed. In this study, BTO was encapsulated, leveraging the macrophages' ability to recognize bacteria, targeting bacterial infection sites. Under ultrasound stimulation, BTO nanoparticles in BTO@MMSa generated local electric fields and surface potentials through the piezo-

electric effect, triggering redox reactions and efficiently producing ROS (Fig. 5B). Furthermore, under low-intensity ultrasound, BTO@MMSa enhanced fibroblast migration, collagen synthesis, and reduced inflammation, thereby promoting wound healing and accelerating the repair of bacterial-infected wounds. Experimental results showed that under ultrasound exposure, BTO@MMSa achieved an antibacterial efficiency of 99.30% against *S. aureus* and 93.40% against *E. coli*. The dual effects of antibacterial activity and wound healing promotion significantly improved the healing of bacterial-infected wounds (1.5 W cm^{-2}, 1 MHz, 15 min).[66]

3.5 Nanomaterials on bulk surface

In SDT, in addition to nanomaterials that inherently exhibit therapeutic effects, nanomaterial coatings are often applied to the surfaces of bulk implants to enhance their performance and achieve infection treatment. For example, in the study by Guan *et al.*, a metal-phosphorus (RP) heterojunction interface material was synthesized, and Ti-RP-SNO material was prepared (Fig. 6A). This material involved further modification of the Ti-RP surface with a thermally controlled NO releasing mesoporous silica nanoparticle (MSN) coating. Under ultrasound stimulation, this material generates ROS *via* the thermoacoustic effect while simultaneously releasing NO to exert a synergistic antibacterial effect. Experimental results demonstrated that after two treatment cycles, the material + ultrasound group achieved an antibacterial efficiency of 99.99% against MRSA, and *in vivo* experiments confirmed its potential for treating bone infections caused by MRSA (1.0 W cm^{-2}, 1 MHz, 25 min).[68]

Furthermore, the efficiency of ROS generation can be enhanced by introducing oxygen vacancies into the coating. Pan *et al.* synthesized aluminum-doped strontium titanate/titanium dioxide nanotubes (Al-$SrTiO_3$/TiO_2 nanotubes, Al-STNT), designed as an ultrasound-responsive nanocoating fixed onto the surface of Ti implants (Fig. 6B). The doping of Al^{3+} ions into the $SrTiO_3$/TiO_2 heterojunction creates oxygen vacancies and disrupts the lattice of $SrTiO_3$. Under ultrasound stimulation, the piezoelectric effect overcomes the bandgap barrier, leading to increased ROS production by Al-STNT. Experimental results demonstrated that this material achieved antibacterial rates of 80.40% and 82.10% against *P. gingivalis* and *F. nucleatum*, respectively (1.5 W cm^{-2},1 MHz, 20 min). *In vivo* experiments confirmed its potential for treating *peri*-implantitis caused by bacterial infections.[69] Similarly, in a study by Chen *et al.*, a bilayer coating material was prepared on titanium, with the inner layer consisting of microporous TiO_2 and the outer layer of nanorod hydroxyapatite (HA) (Fig. 6C). After magnesium thermal reduction treatment, oxygen vacancies were introduced into TiO_2, enhancing its ROS generation efficiency under ultrasound. Additionally, the Mg–O amorphous film that degraded after MT treatment produced OH^-, which consumed H^+, disrupting the proton gradient inside and outside the bacteria, weakening the transmembrane proton motive force (TPMF), and inhibiting bacterial ATP synthesis. This disruption, in synergy with ROS, resulted in antibacterial activity. *In vitro* experiments showed that the antibacterial efficiency against MRSA reached 99.23%, and against *S. aureus* it was 99.87% (1.5 W cm^{-2}, 5 min). Furthermore, *in vivo* experiments confirmed its potential for treating infectious osteoporotic conditions.[70]

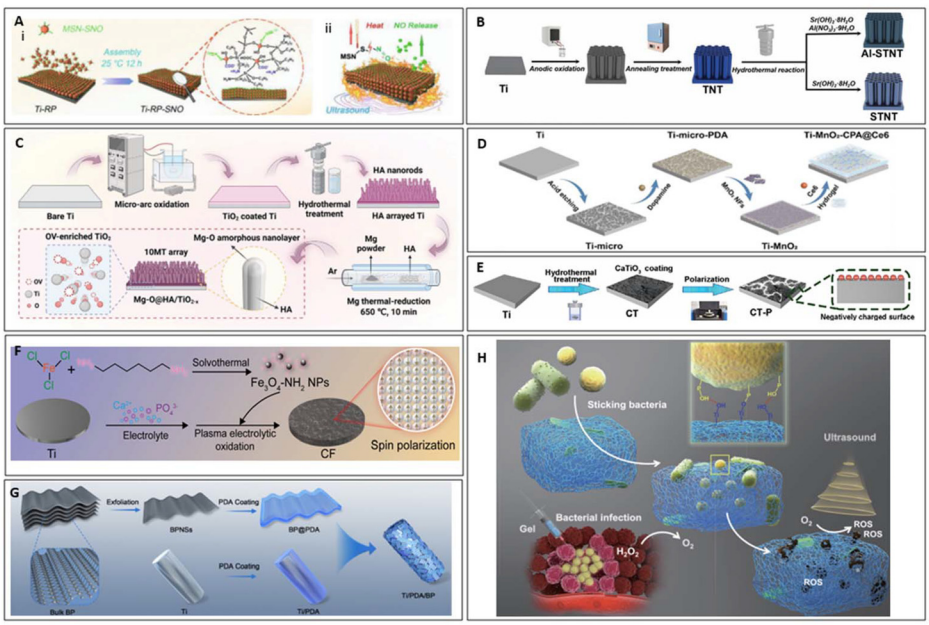

Fig. 6 The preparation of Ti-RP-SNO (A) (i)[68] Copyright©2020, Wiley-VCH, Al-STNT (B)[69] Copyright©2024, Wiley-VCH, 10MT (C)[70] Copyright©2023, Wiley-VCH, Ti-MnO_2-CPA@Ce6 (D)[71] Copyright©2024, Elsevier, CT-P (E)[72] Copyright©2024, Wiley-VCH, CF (F)[73] Copyright©2024, Wiley-VCH, Ti/PDA/BP (G)[43] Copyright©2023, Elsevier. (A) (ii) Mechanism of action of Ti-RP-SNO. (H) Schematic illustration for the functional gel sticking, trapping and killing the bacteria under ultrasound.[74] Copyright©2022, Springer Nature.

Certain nanomaterial coatings can promote the release of modified ions under ultrasound stimulation, thereby achieving the desired therapeutic effects. In the study by Xu *et al.*, a multifunctional coating was constructed on the surface of Ti implants, consisting of MnO_2 nanofibers (MnO_2NFs) and a responsive, biodegradable hydrogel containing Ce6. The Ti-MnO_2-CPA@Ce6 substrate catalyzed hydrogen peroxide generation and, under ultrasound, induced Ce6 to produce ROS for synergistic antibacterial activity (Fig. 6D). Meanwhile, Mn^{2+} released from MnO_2NFs promoted the maturation of dendritic cells (DCs). After bacterial killing, bacterial antigens were released, and the mature DCs enhanced antigen presentation, activated T cells, and induced B cell differentiation into plasma cells, thus initiating adaptive immunity to combat bacterial infections. Experimental results showed significant antibacterial effects against *S. aureus*, and this approach was demonstrated to be useful in treating implant-related infections in diabetic patients, while also promoting bone healing at bone defect sites in these patients (1.5 W cm^{-2}, 20 min).[71]

Some nanomaterials on bulk surfaces can also enhance the electric fields generated by the materials themselves through ultrasound, thereby inducing electrical stimulation to exert their therapeutic effects. Dai *et al.* synthesized a perovskite (CT) coating on Ti through a one-step hydrothermal method, followed by corona polarization treatment to obtain a polarized perovskite (CT-P) coating (Fig. 6E). This coating not only generates ROS under ultrasound but also provides electrical stimulation (ES) to modulate the immune microenvironment. The ES intensity is 0.2 mA, which is much lower than the current intensity typically used for antimicrobial electric fields. Therefore, in this case, it primarily serves to promote immune modulation rather than exerting any direct antimicrobial effects.[75,76] *In vitro*, it regulates the inflammatory response by inhibiting the polarization of pro-inflammatory M1 macrophages and promoting the polarization of anti-inflammatory M2 macrophages. Results showed that the antibacterial efficiency against *S. aureus* reached 90.04 ± 0.04% (1.5 W cm^{-2}, 20 min), and because it can modulate the immune microenvironment to regulate inflammation, it is suitable for treating implant site infections and bone integration failure in oral implant surgeries.[72] Similarly, Ding *et al.*[73] proposed a magnetic heterojunction CF (Fe_3O_4/TiO_2) constructed on the surface of Ti (Fig. 6F). This material generates ROS under ultrasound stimulation to exert antibacterial effects and, through the ferromagnetism of Fe_3O_4, produces spin-polarized electrons that generate a micro-magnetic field. This field disrupts the bacterial respiratory chain, further accelerating bacterial death. Experimental results showed an

Table 1 Antibacterial efficiency of different nanomaterials and the diseases treated. NA indicates that no specific value was provided

Nanomaterials	Classification	Bacteria	Antibacterial efficiency	Treated diseases	Ref.
Sn@hydrogel	2D nanomaterials	MRSA, *S. aureus*	99.80%, 99.50%	Wound infection	47
HNTM/Nb_2C	2D nanomaterials	MRSA	98.64 ± 0.25%	Osteomyelitis	39
TVNMC Mxene	2D nanomaterials	MRSA	99.60%	Wound infection	50
MoS_2	2D nanomaterials	*S. aureus*, *P. aeruginosa*	Nearly 100%	Wound infection	51
Ag@UT	MOFs	*S. aureus*	99%	Wound infection	53
CeTCPP-Au	MOFs	*S. aureus*, *E. coli*	99.73 ± 0.05%, 99.16 ± 0.29%	Osteomyelitis	54
HN25	MOFs	MRSA	98.97%	Osteomyelitis	56
D-PCN-2	Heterojunction	MRSA	93.05%	Osteomyelitis	55
Au-TNT	Heterojunction	*P. gingivalis*, *F. nucleatum*, and *S. sanguinis*	96.59%, 96.25%, and 95.31%	Peri-implant infection	58
S-TiO_{2-x}/CeO_2	Heterojunction	*S. aureus*	99.30%	Osteomyelitis	60
HN-Ti_3C_2	Heterojunction	MRSA	99.75%	Osteomyelitis	38
PtCu-PEG NPs	Heterojunction	*S. aureus*, *E. coli*	99.90%, 99.60%	Wound infection, Osteomyelitis	63
ZnO@HTCS	Heterojunction	MRSA	99.79 ± 0.09%	Osteomyelitis	64
GQD/TiO_{2-x}	Heterojunction	MRSA	NA	Wound infection	42
AB-MN	Others	*S. aureus*	99.94%	Wound infection	65
BTO@MMSa	Others	*S. aureus*, *E. coli*	99.30%, 93.40%	Wound infection	66
Ti-RP-SNO	Nanomaterials on bulk surface	MRSA	99.99%	Osteomyelitis	68
Al-STNT	Nanomaterials on bulk surface	*P. gingivalis*, *F. nucleatum*	80.40%, 82.10%	Peri-implant infection	69
10MT	Nanomaterials on bulk surface	MRSA, *S. aureus*	99.23%, 99.87%	Osteomyelitis	70
Ti-MnO_2-CPA@Ce6	Nanomaterials on bulk surface	*S. aureus*	NA	Bone implant infection	71
CT-P	Nanomaterials on bulk surface	*S. aureus*	90.04 ± 0.04%	Bone implant infection	72
CF	Nanomaterials on bulk surface	*S. aureus*	99.50%	Osteomyelitis	73
Ti/PDA/BP	Nanomaterials on bulk surface	MRSA	96.60%	Bone implant infection	43
Gel	Nanomaterials on bulk surface	MRSA	NA	Wound infection	74

antibacterial efficiency of 99.50% against *S. aureus*, and the material demonstrated efficacy in the treatment of osteomyelitis.

Additional nanoparticles can be modified on bulk surfaces to enable responsiveness to other driving forces, thereby enhancing the antimicrobial efficacy of SDT. In the study by Zeng *et al.*, a bifunctional coating composed of two-dimensional light- and ultrasound-sensitive black phosphorus nanosheets (BPNSs) and polydopamine (PDA) was synthesized and loaded onto Ti implants (Fig. 6G). This material leveraged the combined advantages of photothermal and sonodynamic effects, generating a significant amount of ROS to inactivate *S. aureus*, including MRSA, with an *in vitro* antibacterial rate of 96.60%. In this study, the material was primarily used for treating orthopedic implant-related infections while promoting bone–implant integration, addressing the issue of implant failure.[43]polydopamine (PDA) was synthesized and loaded onto Ti implants. This material leveraged the combined advantages of photothermal and sonodynamic effects, generating a significant amount of ROS to inactivate *S. aureus*, including MRSA, with an *in vitro* antibacterial rate of 96.60% (the ultrasound intensity is 1.5 W cm^{-2}). In this study, the material was primarily used for treating orthopedic implant-related infections while promoting bone–implant integration, addressing the issue of implant failure.[43]

Modification of bulk nanomaterial surfaces with additional nanomaterials can enhance adhesion to bacterial surfaces, thereby facilitating targeted treatment of drug-resistant bacterial infections. In a study conducted by Zhu *et al.*, a functional gel was synthesized using amorphous TiO_x nanofibers dotted with $Ti_2C(OH)_2$ nanosheets. This gel exploits the formation of Ti–O–P bonds between Ti–OH groups in the material and phosphate groups in bacterial cell walls, effectively capturing bacteria[74] (Fig. 6H). Under ultrasound, the semiconductor properties of the material promote the generation of e^-/h^+. The separated electrons and holes react with water molecules and dissolved oxygen to produce various ROS, which then interact with bacteria to achieve sterilization. This research demonstrated significant antibacterial activity against MRSA, showing excellent therapeutic effects in healing wounds infected with MRSA (1.0 W cm^{-2}, 1 MHz, 4 min).

4. Conclusions and future challenges

In summary, given the current overuse of antibiotics, there is an urgent need to develop alternative treatments for bacterial infections. Compared to traditional antibiotic therapies, antibiotic-free approaches that generate ROS, particularly those mediated by nanomaterials in SDT, warrant significant attention. This strategy not only avoids the common side effects and resistance issues associated with conventional antibiotics but also provides the flexibility to tailor materials for specific therapeutic purposes. The various materials discussed in this review—including two-dimensional materials, metal–organic frameworks, heterojunction materials, metal oxides, piezoelectric materials, and nanomaterials on bulk surface—respond to ultrasound and generate ROS, offering valuable insights into antimicrobial treatments for a wide range of infectious diseases (Table 1). Compared to other non-antibiotic therapies, SDT offers superior tissue penetration capabilities. This enables higher selectivity at antibacterial targets through the use of specific sonosensitizers. Unlike PDT, which is limited by the need for external light sources, SDT uses ultrasound as an excitation source, allowing for deeper tissue penetration and effective treatment of infections in hard-to-reach areas. Moreover, unlike CDT, which relies on external chemical agents, SDT reduces potential toxicity and resistance issues, making it more advantageous for clinical applications. SDT can also be synergistically combined with other treatment modalities, such as photothermal therapy and chemotherapy, to enhance therapeutic outcomes. As a non-invasive approach, SDT minimizes physical trauma and promotes rapid recovery, avoiding the risks and complications associated with surgery. This makes it a safer and more convenient treatment option for patients who are ineligible for surgery or have other health concerns. These advantages position SDT as an innovative and effective alternative in the fields of infection management and cancer therapy.

However, despite the promising potential of SDT in generating ROS for antibacterial applications, several challenges remain in clinical practice. (1) While ROS can effectively eliminate bacteria, excessive ROS may also cause oxidative damage to host cells, leading to cell death or dysfunction. Therefore, it is critical to investigate the interactions between nanomaterials, cells, biomolecules, and biological membranes, particularly within the context of ROS-mediated antimicrobial processes. Understanding how these interactions influence ROS generation and antimicrobial efficacy, as well as their potential impact on surrounding healthy cells, is essential for precisely controlling the intensity and duration of ultrasound to prevent damage to healthy tissues. Future research should focus on exploring strategies to regulate ROS production during antimicrobial treatments based on specific conditions, as well as investigating the use of low-intensity, high-frequency ultrasound to minimize the effects on surrounding healthy tissue. (2) The effectiveness of ultrasound may be influenced by factors such as tissue structure, bacterial biofilm barriers, and the viscosity of the medium. For instance, ultrasound may fail to penetrate thick biofilms effectively, thereby limiting its antimicrobial efficacy. Future studies should explore the surface modification of materials with nanoparticles that exhibit penetrating or anti-biofilm properties, or the incorporation of targeting ligands, to enhance material affinity for biofilms and improve treatment outcomes. (3) As with other clinical materials, the biocompatibility and toxicity of these nanomaterials remain important concerns, especially with prolonged use. Addressing the accumulation and toxicity of nanomaterials in the body is crucial to prevent adverse effects on patient health. (4) The translation of materials from synthesis to clinical application must be accelerated. Collaborative efforts with clinical therapies are essential for developing

nanomaterials that meet biomedical needs and have practical application potential, thereby facilitating the transition of SDT from laboratory research to clinical practice. We believe that solving these challenges will pave the way for the development of a new field of antibiotic-free bacterial infection treatments.

Author contributions

Gaoquan Zheng: methodology, data curation, visualization, writing – original draft. Zhongmin Tang: funding acquisition, validation, supervision, writing – review & editing. Feng Peng: funding acquisition, supervision, methodology, writing – review & editing.

Data availability

Data available on request from the authors.

Conflicts of interest

There are no conflicts to declare.

Acknowledgements

This work was supported by the National Natural Science Foundation of China (52371252), the Natural Science Foundation of Guangdong Province, China (2023A1515012901) and Fundamental Research Funds for the Central Universities.

References

1 S. Dhingra, N. A. A. Rahman, E. Peile, M. Rahman, M. Sartelli, M. A. Hassali, T. Islam, S. Islam and M. Haque, *Front. Public Health*, 2020, **8**, 535668.
2 B. Spellberg, J. Bartlett, R. Wunderink and D. N. Gilbert, *Am. J. Respir. Crit. Care Med.*, 2015, **191**, 135–140.
3 I. D. S. O. America, *Clin. Infect. Dis.*, 2008, **47**, S249–S265.
4 D. L. Paterson and P. N. A. Harris, *Lancet Infect. Dis.*, 2016, **16**, 132–133.
5 T. A. Wencewicz, *J. Mol. Biol.*, 2019, **431**, 3370–3399.
6 L. Han, Z. Yuan, H.-M. Ren, W. Song, R. Wu, J. Li, Z. Guo, B. Yu, S. Duan and F.-J. Xu, *BMEMat*, 2024, **2**, e12082.
7 S. McCallin, T. M. Kessler and L. Leitner, *Clin. Microbiol. Infect.*, 2023, **29**, 1267–1271.
8 S. Sabbatini, C. Monari, N. Ballet, P. Mosci, A. C. Decherf, F. Pélerin, S. Perito, P. Scarpelli and A. Vecchiarelli, *Virulence*, 2018, **9**, 954–966.
9 T. Pan, B. Heng, Y. Li, X. Zhang and X. Deng, *Chin. J. Dent. Res.*, 2020, **23**, 235–255.
10 Z.-Y. Liu, X.-Y. Tang, C.-Q. Huang, J. Zhang, W.-Q. Huang and Y. Ye, *Inorg. Chem. Front.*, 2022, **9**, 1836–1846.
11 X. Xie, W. Gao, J. Hao, J. Wu, X. Cai and Y. Zheng, *J. Nanobiotechnol.*, 2021, **19**, 126.
12 C. He, P. Feng, M. Hao, Y. Tang, X. Wu, W. Cui, J. Ma and C. Ke, *Adv. Funct. Mater.*, 2024, **34**, 2402588.
13 Z. Qiao, K. Zhang, J. Liu, D. Cheng, B. Yu, N. Zhao and F.-J. Xu, *Nat. Commun.*, 2022, **13**, 7164.
14 Q. Li, Y. Zhang, X. Huang, D. Yang, L. Weng, C. Ou, X. Song and X. Dong, *Chem. Eng. J.*, 2021, **407**, 127200.
15 M. Zhang, S. Ran, X. Yin, J. Zhang, X. Sun, W. Sun and Z. Zhu, *BMEMat*, 2023, **1**, e12041.
16 J. Roy, V. Pandey, I. Gupta and H. Shekhar, *ACS Biomater. Sci. Eng.*, 2021, **7**, 5326–5338.
17 Y. Qi, K. Qian, J. Chen, Y. E. Y. Shi, H. Li and L. Zhao, *J. Nanobiotechnol.*, 2021, **19**, 414.
18 C. Dong, W. Fang, Q. Yi and J. Zhang, *Chemosphere*, 2022, **308**, 136205.
19 Z. Yang, Z. Min and B. Yu, *Int. Rev. Immunol.*, 2020, **39**, 292–298.
20 F. C. Fang, *mBio*, 2011, **2**, 5.
21 C. Elian, R. Méallet and D.-L. Versace, *Adv. Funct. Mater.*, 2024, **34**, 2407228.
22 J. Laval, *Pathol. Biol.*, 1996, **44**, 14–24.
23 M. M. Fetherolf, S. D. Boyd, D. D. Winkler and D. R. Winge, *Metallomics*, 2017, **9**, 1047–1059.
24 N. Paillous and S. Fery-Forgues, *Biochimie*, 1994, **76**, 355–368.
25 C. Lee, M. Park, W. C. B. Wijesinghe, S. Na, C. G. Lee, E. Hwang, G. Yoon, J. K. Lee, D.-H. Roh, Y. H. Kwon, J. Yang, S. A. Hughes, J. E. Vince, J. K. Seo, D. Min and T.-H. Kwon, *Nat. Commun.*, 2024, **15**, 4025.
26 N. Afshan, R. Tariq, I. Riaz, A. Manan, A. Iqbal, M. Ejaz, A. Sohail, A. Bari, S. Mahmood, S. Iqbal, K. M. Alotaibi and M. Alshalwi, *J. Chem. Technol. Biotechnol.*, 2024, **99**, 2027–2034.
27 S.-C. Park, N.-H. Kim, W. Yang, J.-W. Nah, M.-K. Jang and D. Lee, *J. Controlled Release*, 2016, **221**, 37–47.
28 A. Müller, A. Preuß and B. Röder, *J. Photochem. Photobiol., B*, 2018, **178**, 219–227.
29 J. Regensburger, T. Maisch, A. Felgenträger, F. Santarelli and W. Bäumler, *J. Biophotonics*, 2010, **3**, 319–327.
30 T. Maisch, J. Baier, B. Franz, M. Maier, M. Landthaler, R.-M. Szeimies and W. Bäumler, *Proc. Natl. Acad. Sci. U. S. A.*, 2007, **104**, 7223–7228.
31 J. Xiao, S. Guo, D. Wang and Q. An, *Chem. – Eur. J.*, 2024, **30**, e202304337.
32 J. Sun, S. Gao, G. Wei, S. Yu, S. Zhang, A. Yang and W. Lu, *Nano Lett.*, 2024, **25**(1), 343–352.
33 R. Zhao, J. Li, K. Wei, X. Lei, Y. Li, Y. Liu, W. Gong, J. Lv and J. Jia, *Sep. Purif. Technol.*, 2025, **355**, 129793.
34 Y. Hong, Q. Li, Q. Gao, J. Xie, H. Huang, K. Drlica and X. Zhao, *J. Antimicrob. Chemother.*, 2019, **75**, 576–585.
35 F. B. Rashed, W. D. Kate, M. Fanta, L. I. Wiebe, P. Kumar and M. Weinfeld, *Antioxidants*, 2023, **12**, 389.
36 C. Li, F. Teng, F. Wu, H. Zhang, C. Zhang and D. Zhang, *Ultrason. Sonochem.*, 2024, **105**, 106853.

37 S. Wu, Q. Wang, J. Du, L. Zhu, F. Yang, J. Lu, X. Li, Y. Li, J. Cui and Y. Miao, *Adv. Healthcare Mater.*, 2024, **13**, 2401697.
38 H. Wang, N. Mu, Y. He, X. Zhang, J. Lei, C. Yang, L. Ma and Y. Gao, *Theranostics*, 2023, **13**, 1669–1683.
39 L. Ma, X. Zhang, H. Wang, X. Feng, J. Lei, Y. He, J. Wei, Y. Zhang, L. Tan and C. Yang, *Sci. China Mater.*, 2023, **66**, 2913–2924.
40 L. Wang, Y. Li, L. Zhao, Z. Qi, J. Gou, S. Zhang and J. Z. Zhang, *Nanoscale*, 2020, **12**, 19516–19535.
41 X. Xiao, Y. Zhao, P. A. Ma, Z. Cheng and J. Lin, *Chem. Eng. J.*, 2022, **440**, 135812.
42 Y. Qian, J. Wang, X. Geng, B. Jia, L. Wang, Y.-Q. Li, B. Geng and W. Huang, *Adv. Healthcare Mater.*, 2024, **13**, 2400659.
43 J. Zeng, C. Gu, X. Geng, K. Lin, Y. Xie and X. Chen, *Biomaterials*, 2023, **297**, 122122.
44 X. Yang, J. Li, T. Liang, C. Ma, Y. Zhang, H. Chen, N. Hanagata, H. Su and M. Xu, *Nanoscale*, 2014, **6**, 10126–10133.
45 Y. Yu, L. Lu, Q. Yang, A. Zupanic, Q. Xu and L. Jiang, *ACS Appl. Nano Mater.*, 2021, **4**, 7523–7537.
46 X. Wang, Y. Shao, C. Yao, L. Huang, W. Song, X. Yang and Z. Zhang, *J. Colloid Interface Sci.*, 2025, **678**, 30–41.
47 N. Tao, Z. Zeng, Y. Deng, L. Chen, J. Li, L. Deng and Y.-N. Liu, *Chem. Eng. J.*, 2023, **456**, 141109.
48 W. Chen, C. Liu, X. Ji, J. Joseph, Z. Tang, J. Ouyang, Y. Xiao, N. Kong, N. Joshi, O. C. Farokhzad, W. Tao and T. Xie, *Angew. Chem., Int. Ed.*, 2021, **60**, 7155–7164.
49 Y. Yu, H. Sun, Q. Lu, J. Sun, P. Zhang, L. Zeng, K. Vasilev, Y. Zhao, Y. Chen and P. Liu, *J. Nanobiotechnol.*, 2023, **21**, 193.
50 W. Song, D. Wang, S. Xiao, X. He, W. Xiong and J. Shen, *Mater. Des.*, 2024, **240**, 112857.
51 H. Chen, X. He, Z. Zhou, Z. Wu, H. Li, X. Peng, Y. Zhou, C. Tan and J. Shen, *J. Nanobiotechnol.*, 2022, **20**, 136.
52 S. Dang, Q.-L. Zhu and Q. Xu, *Nat. Rev. Mater.*, 2017, **3**, 17075.
53 L. Ma, Y. Cheng, X. Feng, X. Zhang, J. Lei, H. Wang, Y. Xu, B. Tong, D. Zhu, D. Wu, X. Zhou, H. Liang, K. Zhao, K. Wang, L. Tan, Y. Zhao and C. Yang, *Adv. Mater.*, 2024, **36**, 2307846.
54 S. Sun, X. Meng, J. Xu, Z. Yang, X. Zhang and H. Dong, *Nano Today*, 2024, **55**, 102181.
55 Q. Zheng, X. Liu, S. Gao, Z. Cui, S. Wu, Y. Liang, Z. Li, Y. Zheng, S. Zhu, H. Jiang and R. Zou, *Small*, 2023, **19**, 2207687.
56 F. Wang, B. Wang, W. You, G. Chen and Y.-Z. You, *Nano Res.*, 2022, **15**, 9223–9233.
57 F. Li, Q. Pan, Y. Ling, J. Guo, Y. Huo, C. Xu, M. Xiong, M. Yuan, Z. Cheng, M. Liu and J. Lin, *Chem. Eng. J.*, 2023, **460**, 141791.
58 G. Li, S. Wu, J. Liu, K. Wang, X. Chen and H. Liu, *Adv. Mater.*, 2024, **36**, 2401252.
59 C. Wang, J. Lei, C. Mao, S. Wu, Y. Zheng, C. Liang, L. Yang, S. Zhu, Z. Li, H. Jiang, Y. Zhang, C. Yang and X. Liu, *Adv. Funct. Mater.*, 2023, **33**, 2306493.
60 S.-L. Li, H.-L. Dong, H.-Y. Hou, X. Chu, H. Chen, Y. Sun and Y. Liu, *Int. J. Biol. Macromol.*, 2024, **258**, 129120.
61 F. Qi, Z. Li, H. Li, G. Chen, X. Luo, S. Xiong, S. Peng, H. Zhu and C. Shuai, *Vacuum*, 2023, **216**, 112433.
62 Y. Zeng, Q. Ouyang, Y. Yu, L. Tan, X. Liu, Y. Zheng and S. Wu, *Small Methods*, 2023, **7**, 2201248.
63 S. Cheng, L. Chen, F. Gong, X. Yang, Z. Han, Y. Wang, J. Ge, X. Gao, Y. Li, X. Zhong, L. Wang, H. Lei, X. Zhou, Z. Zhang and L. Cheng, *Adv. Funct. Mater.*, 2023, **33**, 2212489.
64 Y. Guo, C. Mao, S. Wu, C. Wang, Y. Zheng and X. Liu, *Small*, 2024, **20**, 2400732.
65 Q. Ouyang, Y. Zeng, Y. Yu, L. Tan, X. Liu, Y. Zheng and S. Wu, *Small*, 2023, **19**, 2205292.
66 X. Qian, T. Lu, C. Huang, D. Zheng, G. Gong, X. Chu, X. Wang, H. Lai, L. Ma, L. Jiang, X. Sun, X. Ji, M. Li and Y. Zhang, *Adv. Funct. Mater.*, 2024, **34**, 2315576.
67 Y. Zhao, T. Huang, X. Zhang, Y. Cui, L. Zhang, L. Li and Z. L. Wang, *BMEMat*, 2023, **1**, e12006.
68 W. Guan, L. Tan, X. Liu, Z. Cui, Y. Zheng, K. W. K. Yeung, D. Zheng, Y. Liang, Z. Li, S. Zhu, X. Wang and S. Wu, *Adv. Mater.*, 2021, **33**, 2006047.
69 Q. Pan, Y. Zheng, Y. Zhou, X. Zhang, M. Yuan, J. Guo, C. Xu, Z. Cheng, A. A. A. Kheraif, M. Liu and J. Lin, *Adv. Funct. Mater.*, 2024, **34**, 2313553.
70 S. Chen, F. Liu, H. Xin, D. Wen, Y. Zhang, B. Li and Y. Han, *Adv. Funct. Mater.*, 2024, **34**, 2311965.
71 K. Xu, Y. Zou, C. Lin, L. Zhang, M. Tan, M. Li, J. Wu, X. Li, Y. He, P. Liu, K. Li and K. Cai, *Biomaterials*, 2024, **311**, 122649.
72 X. Dai, T. Li, P. Wei, Y. Xu, C. Jiang, X. Zhang, X. Zhang, L. Liao and X. Wang, *Small*, 2024, 2403298.
73 T. Ding, Y. Li, F. Liu, J. Chen, Y. Chen, L. Kong, Y. Han and L. Zhang, *Adv. Funct. Mater.*, 2024, **34**, 2401795.
74 Y.-Q. Zhu, W.-Q. Huang, G. Chen, L. Xia, Y.-Z. You and Y. Yu, *Nano Res.*, 2022, **15**, 9105–9113.
75 Q. Yang, R. Chen, M. Li, H. Song, X. Zhao, L. Zhang, Y. Zhou, J. Chen, J. Li and M. Chen, *Adv. Funct. Mater.*, 2025, **35**, 2413080.
76 R. V. Badhe, A. Godse, A. Shinkar, A. Kharat, V. Patil, A. Gupta and S. Kheur, *Turk. J. Pharm. Sci.*, 2021, **18**, 483–491.